

Article

Adsorption Characteristics of Phosphate Ions by Pristine, CaCl₂ and FeCl₃-Activated Biochars Originated from Tangerine Peels

Changgil Son ¹, Wonyeol An ², Geonhee Lee ², Inho Jeong ², Yong-Gu Lee ^{2,*} and Kangmin Chon ^{1,2,*} 

¹ Department of Integrated Energy and Infra System, Kangwon National University, Kangwondaehak-gil, 1, Chuncheon-si, Gangwon-do 24341, Korea; soncgrs@gmail.com

² Department of Environmental Engineering, College of Engineering, Kangwon National University, Kangwondaehak-gil, 1, Chuncheon-si, Gangwon-do 24341, Korea; newtree1046@gmail.com (W.A.); ksjun5@naver.com (G.L.); jih5742@naver.com (I.J.)

* Correspondence: yglee19@kangwon.ac.kr (Y.-G.L.); kmchon@kangwon.ac.kr (K.C.); Tel.: +82-33-250-6352 (K.C.)

Abstract: This study has evaluated the removal efficiencies of phosphate ions (PO₄³⁻) using pristine (TB) and chemical-activated tangerine peel biochars. The adsorption kinetics and isotherm presented that the enhanced physicochemical properties of TB surface through the chemical activation with CaCl₂ (CTB) and FeCl₃ (FTB) were helpful in the adsorption capacities of PO₄³⁻ (equilibrium adsorption capacity: FTB (1.655 mg g⁻¹) > CTB (0.354 mg g⁻¹) > TB (0.104 mg g⁻¹)). The adsorption kinetics results revealed that PO₄³⁻ removal by TB, CTB, and FTB was well fitted with the pseudo-second-order model (R² = 0.999) than the pseudo-first-order model (R² ≥ 0.929). The adsorption isotherm models showed that the Freundlich equation was suitable for PO₄³⁻ removal by TB (R² = 0.975) and CTB (R² = 0.955). In contrast, the Langmuir equation was proper for PO₄³⁻ removal by FTB (R² = 0.987). The PO₄³⁻ removal efficiency of CTB and FTB decreased with the ionic strength increased due to the compression of the electrical double layer on the CTB and FTB surfaces. Besides, the PO₄³⁻ adsorptions by TB, CTB, and FTB were spontaneous endothermic reactions. These findings demonstrated FTB was the most promising method for removing PO₄³⁻ in waters.

Keywords: adsorption; biochar; chemical activation; phosphate ions; tangerine peel



Citation: Son, C.; An, W.; Lee, G.; Jeong, I.; Lee, Y.-G.; Chon, K. Adsorption Characteristics of Phosphate Ions by Pristine, CaCl₂ and FeCl₃-Activated Biochars Originated from Tangerine Peels. *Separations* **2021**, *8*, 32. <https://doi.org/10.3390/separations8030032>

Academic Editor: Giusy Lofrano

Received: 29 January 2021

Accepted: 10 March 2021

Published: 13 March 2021

Publisher's Note: MDPI stays neutral with regard to jurisdictional claims in published maps and institutional affiliations.



Copyright: © 2021 by the authors. Licensee MDPI, Basel, Switzerland. This article is an open access article distributed under the terms and conditions of the Creative Commons Attribution (CC BY) license (<https://creativecommons.org/licenses/by/4.0/>).

1. Introduction

With a significant increase in the amount of nutrients introduced to the water system due to the rapid industrialization and recent population growth, increasing water pollution hinders effective water quality management [1,2]. Nutrients are divided into point and non-point sources, depending on the primary source of inflow. Although most effluents from domestic sewage treatment plants and livestock wastewater treatment plants meet the water quality criteria, agricultural drainage water, a representative non-point source, significantly affects the discharge of nutrients because the increased amounts of compost or fertilizer used to improve agricultural production [3,4]. This oversupply of nutrients into the water system through point and non-point sources increases eutrophication causes algal blooms. It reduces the amount of dissolved oxygen in the aquatic ecosystem, thereby causing the deaths of aquatic organisms [5]. Among the main components of nutrients, nitrate ions (NO₃⁻) are required in relatively large quantities for algal growth, but phosphate ions (PO₄³⁻) are a limiting factor that can promote algal growth even when present in small amounts. PO₄³⁻ can lead to blue-green algal blooms, leading to renal failure through toxicity [6,7].

The anaerobic anoxic aerobic (A2O) process is typically applied for the biological treatment of PO₄³⁻. Although this process requires no chemical injection and generates little sludge compared to the amount of phosphate removed [8], the results are significantly affected by the operating conditions. Besides, A2O is not suitable for strict water quality

criteria because it cannot protect microorganisms against toxic chemicals present in the influent water. Moreover, microorganisms in the A2O process are subject to more significant technical limitations in treatment efficiency compared with the physicochemical treatment process [6]. There are commonly used physicochemical treatment processes (e.g., Electrodialysis, membrane filtration, coagulation, precipitation, and adsorption) to remove PO_4^{3-} from water and wastewater treatment plants [9]. These techniques are not appropriate to the full-scale water and wastewater treatment plants due to the high operating costs and energy consumption [10], and the generated sludge may cause secondary environmental pollution in subsequent treatment processes [11]. However, the adsorption process has been used in the water and wastewater treatment plants due to low operation and maintenance costs [12]. The various types of PO_4^{3-} adsorbents, such as clay minerals [13], fly ashes [14], and metal oxides [15], have been investigated. Das et al. have demonstrated the high PO_4^{3-} adsorption on clay minerals, including layered double hydroxides [13]. Chen et al. reported the efficient PO_4^{3-} adsorption on fly ashes [14]. Zhang et al. have fabricated activated carbon fiber with metal oxides for PO_4^{3-} adsorption [15]. Despite the advantage of these adsorbents, including high efficiency and environment-friendly properties, they were difficult to be applied the full-scale wastewater treatment plant for PO_4^{3-} adsorption due to the high treatment cost (e.g., recycle and regeneration). Therefore, it was necessary to develop an alternative adsorbent to remove PO_4^{3-} in water [16].

Biochars, alternative adsorbents, are carbon-rich substances obtained through biomass pyrolysis, such as fruit peels and rice bran, under oxygen-limited conditions. The utilization of biochar shows significant environmental advantages in reducing greenhouse gas emissions and resource recycling technology of agriculture and food residues [17]. The agricultural residues represent an important potential source of reusable products [18,19]. Tangerine peels are common agricultural residues in Korea. The amount of tangerines produced in Jeju Island was 125,343 tons as of 2005, representing approximately 18% of the total global tangerine production. Annually, over 55,000 tons have been discarded as tangerine peels [20]. Tangerine peels can be highly applicable as a raw material for biochars because they are mainly composed of pectin, hemicellulose, and cellulose substances [21,22]. The negative surface charge of pristine biochar has limited their adsorption affinity towards anions, including PO_4^{3-} [23,24]. Therefore, their adsorption capacities might be considerably enhanced after modification, including chemical activation, surface functionality modification, and biochar impregnated with metals (e.g., CaCl_2 , MgCl_2 , FeCl_3 , and AlOOH) [24–28]. Fang et al. have demonstrated the high PO_4^{3-} adsorption on MgCl_2 modified ground corn biochar [27]. Zhang and Gao. have reported the efficient PO_4^{3-} adsorption on AlOOH modified cottonwood biochar [24]. Despite the effective adsorption capacities of metal-loaded biochar for PO_4^{3-} , these biochars preparation demanded high energy for pyrolysis, and the adsorption ability of biochars reduced due to coalescence with water [24,27]. CaCl_2 and FeCl_3 , which are a type of chemical coagulants, are commonly used in the adsorption of PO_4^{3-} in water. Thus, the modification of biochars with CaCl_2 and FeCl_3 could significantly improve the adsorption capacities of PO_4^{3-} in water.

The primary purpose of this study is to evaluate the effect of pretreatment with CaCl_2 and FeCl_3 on the PO_4^{3-} removal of biochars made from tangerine peels. Thus, the effects of various conditions, such as the biochar dosage, pH, ionic strength, and temperature, on PO_4^{3-} removal were evaluated using the pristine tangerine peel biochar (TB), and CaCl_2 (CTB) and FeCl_3 (FTB) activated tangerine peel biochars. In addition, the PO_4^{3-} adsorption mechanisms of TB, CTB, and FTB were investigated through adsorption kinetics and adsorption isotherm models.

2. Materials and Methods

2.1. Chemicals and Reagents

Potassium dihydrogen phosphate (KH_2PO_4 , 99.0%), CaCl_2 (>99.0%), FeCl_3 (>99.0%), sodium chloride (NaCl , 99.0%), sodium hydroxide (NaOH , 99.0%), and hydrochloric acid (HCl , 35%) were purchased from Daejung Chemicals (Siheung-si, Gyeonggi-do,

Korea). All chemicals were used without further purification. Deionized (DI) water (resistivity > 18.2 M Ω cm⁻¹, Barnstead Nanopure Water System, Lake Balboa, CA, USA) was applied to make the PO₄³⁻ stock solution (concentration = 10 mg L⁻¹).

2.2. Preparation of Tangerine Peel Biochars

Tangerine peels were purchased from a local food store on Jeju Island (Jeju-do, Korea). After dried tangerine peels were crushed to 0.5–1.0 mm using a blender, they were several rinsed (ten times) with DI water to remove impurities and then dried in an oven at 105 °C for 12 h. The crushed tangerine peels were immersed in 200 mL solutions of 1 M CaCl₂ and 1 M FeCl₃, respectively. They were then stirred at 80 °C for 1 h and dried in an oven at 105 °C for 24 h. The pristine and chemical activated tangerine peels were pyrolyzed at 800 °C for 1 h using a tubular furnace (PyroTech, Namyangju, Gyeonggi-do, Korea) under N₂ gas (the flow rate = 0.25 L min⁻¹) atmospheric conditions (heating rate = 5 °C min⁻¹) [29]. After cooling to room temperature (20 ± 0.5 °C), the fabricated tangerine peel biochars were rinsed using DI water until no impurities were observed and dried in an oven at 80 °C for 24 h. The dried tangerine peel biochars (i.e., TB, CTB, and FTB) were sieved to obtain a homogenized particle size of 150 μ m and then stored in a desiccator prior to use.

2.3. Characteristics of Tangerine Peel Biochars

Total carbon (C), nitrogen (N), and hydrogen (H) contents of the pristine and chemical activated tangerine peel biochars were analyzed using a CHN element analyzer (Flash 2000, Thermo Fisher, Waltham, MA, USA). The average pore size (nm) and specific surface area (m² g⁻¹) were measured using a Brunauer–Emmett–Teller (BET; BELSORP-mini II, Microtrac BEL, Osaka, Japan) analyzer. An X-ray diffractometer (XRD; D/Max-2500, Rigaku, Tokyo, Japan) was used to analyze the surface crystallinity of TB, CTB, and FTB. The surface morphologies of TB, CTB, and FTB were observed using a ultra-high resolution scanning electron microscope (UH-SEM; S-4800, Hitachi, Tokyo, Japan), and the atomic-resolution chemical mapping of calcium and iron ions were identified using energy-dispersive X-ray spectroscopy (EDX; Link ISIS 300, Oxford Instruments, Abingdon, UK).

2.4. Adsorption Experiments

2.4.1. Optimal Dosage

The adsorption of PO₄³⁻ was examined to determine the optimal adsorbent dosages of TB, CTB, and FTB. Each adsorbent dosage (TB = 0.2–2.0 g L⁻¹; CTB = 0.2–12 g L⁻¹; FTB = 0.2–2.0 g L⁻¹) was added to Erlenmeyer flasks containing 25 mL of the PO₄³⁻ solution (initial concentration = 1 mg L⁻¹, pH = 7.0) The sample solutions were stirred at 25 °C and 150 rpm for 24 h using a shaking incubator (VS-8480, Vision Scientific, Daejeon-Si, Korea). Upon completing the adsorption experiment, the sample solutions were filtered using a glass fiber filter (GF/F, Whatman, Maidstone, UK) with a nominal pore size of 0.7 μ m to remove adsorbents. The PO₄³⁻ concentration was analyzed at UV absorbances of 880 nm using the ascorbic acid method (UV-Vis Spectrophotometer, UV-1280, Shimadzu, Kyoto, Japan) [30]. The experiment was performed in triplicate to minimize errors.

2.4.2. Adsorption Kinetics

The adsorption kinetics was conducted by adding the optimal dosage of each TB, CTB, and FTB to Erlenmeyer flasks containing 25 mL of the PO₄³⁻ solution (initial concentration = 1 mg L⁻¹, pH = 7.0). The sample solutions were stirred at 150 rpm during a certain period (0.5–48 h) at 25 °C in a shaking incubator. After the adsorption kinetics experiment, the sample solutions were filtered using GF/F. The concentrations of PO₄³⁻ at the initial and equilibrium states were measured using a UV-Vis spectrophotometer. The experiment was performed in triplicate to minimize errors. All adsorption experiments are repeated three times to minimize errors. The amount of PO₄³⁻ adsorbed per unit mass

of the TB, CTB, and FTB at equilibrium, Q_e (mg g^{-1}), was calculated using the following Equation (1):

$$Q_e = \frac{(C_0 - C_e)V}{M} \tag{1}$$

where V is the volume of the solution (L). C_0 and C_e are the initial and equilibrium concentrations of PO_4^{3-} solution (mg L^{-1}), and M (g) is the mass of the used adsorbent.

The PO_4^{3-} removal efficiency was calculated using Equation (2):

$$\text{Removal efficiency of phosphate ions (\%)} = \frac{(C_0 - C_e)V}{C_0} \times 100 \tag{2}$$

The PO_4^{3-} adsorption characteristics and adsorption capacity of each TB, CTB, and FTB were investigated using the following Equations (3) and (4) [31]:

$$\text{Pseudo-first-order model : } Q_t = Q_e \left(1 - e^{-k_1 t}\right) \tag{3}$$

$$\text{Pseudo-second-order model : } Q_t = \frac{k_2 Q_e^2 t}{1 + k_2 Q_e t} \tag{4}$$

where Q_t (mg g^{-1}) is the amount of the adsorbed PO_4^{3-} on the TB, CTB, and FTB at the time t , t (min) is the adsorption time. k_1 (min^{-1}) is the constant of the pseudo-first-order model and k_2 ($\text{g mg}^{-1} \cdot \text{min}$) is the constant of the pseudo-second-order model.

2.4.3. Adsorption Isotherm

To investigate the adsorption isotherm of PO_4^{3-} by TB, CTB, and FTB, the adsorption isotherm experiment was performed by adjusting the PO_4^{3-} concentrations ($0.5\text{--}10 \text{ mg L}^{-1}$) and adding each optimal adsorbent dosage under controlled conditions (agitation speed = 150 rpm, contact time = 24 h, pH = 7.0, and temperature = 25 °C). The adsorption isotherm results were analyzed using the Langmuir isotherm and Freundlich isotherm models [32].

$$\text{Langmuir Isotherm : } Q_e = \frac{Q_{max} K_L C_e}{1 + K_L C_e} \tag{5}$$

where Q_{max} (mg g^{-1}) is the maximum adsorption capacity in the Langmuir isotherm model, and K_L (L mg^{-1}) is the equilibrium constant of the linearized Langmuir isotherm model. $R_L = 1/(1 + K_L C_0)$, derived from K_L , can be used to compare the adsorption affinity of Langmuir isotherms [33]:

$$\text{Freundlich isotherm : } Q_e = K_F C_e^{1/n} \tag{6}$$

where K_F ($\text{mg}^{-1/n} \text{L}^{1/n} \text{g}^{-1}$) is the Freundlich isotherm adsorption constant related to the relative maximum adsorption capacity, and n is the dimensionless adsorption intensity.

2.4.4. Effects of pH and Ionic Strength

The effects of pH and ionic strength on the adsorptions of the PO_4^{3-} by the TB, CTB, and FTB were evaluated by adjusting solution pH (pH = 3.0–9.0) and ionic strengths (ionic strength = 0–0.5 M) using 0.1 N HCl and 0.1 N NaOH, and NaCl, respectively (initial concentration of PO_4^{3-} solution = 1 mg L^{-1} , agitation speed = 150 rpm, contact time = 24 h). The removal efficiencies of PO_4^{3-} using TB, CTB, and FTB were calculated by Equation (2).

2.4.5. Effects of Temperature

The effects of the temperature of the solution on the PO_4^{3-} removal efficiency of the TB, CTB, and FTB were performed under various temperature (15–35 °C) conditions (initial concentration of PO_4^{3-} solution = 1 mg L^{-1} , agitation speed = 150 rpm, contact time = 24 h,

and pH 7.0). The removal efficiencies of PO₄³⁻ using TB, CTB, and FTB were followed by Equation (2).

The thermodynamic parameters of the PO₄³⁻ adsorption are calculated using the following Equations (7)–(9) [34]:

$$K_d = \frac{Q_e}{C_e} \tag{7}$$

$$\Delta G^\circ = -RT \ln(1000K_d) \tag{8}$$

$$\ln(1000K_d) = \frac{\Delta S^\circ}{R} - \frac{\Delta H^\circ}{RT} \tag{9}$$

where K_d (L g⁻¹) is the partition coefficient. ΔG° in (kJ mol⁻¹), ΔH° in (kJ mol⁻¹), and ΔS° in (J mol⁻¹·K) are the Gibbs free energy, enthalpy, and entropy, respectively. R is the ideal gas constant (8.314 J mol⁻¹·K), and T is the absolute temperature (K). ΔH° and ΔS° were calculated as the slope and intercept in the linear graph of $\ln K_d$ and $1/T$, respectively.

3. Results and Discussions

3.1. Characterization of TB, CTB, and FTB

3.1.1. Elemental Composition and Functionality Analyses

The elemental composition (i.e., C, H, O, and N) and surface properties (i.e., specific surface area pore volume and average pore size) of TB, CTB, and FTB associated with the adsorption capacity of PO₄³⁻ are presented in Table 1. Although the H (TB: 1.50%, CTB: 1.94%, and FTB: 1.63%) and N (TB: 2.09%, CTB: 1.31%, and FTB: 1.05%) contents of TB, CTB and FTB were similar, CTB and FTB had lower C (CTB: 69.42% and FTB: 53.81%) content and higher O (CTB: 7.61% and FTB: 8.39%) content than those of TB (C content = 81.12%, O content = 4.40%). The atomic ratios of H/C, O/C, and (O + N)/C are generally distinguished for carbonization, surface hydrophobicity, and polarity, respectively [35]. The CTB and FTB showed higher values of the H/C (CTB: 0.34 and FTB: 0.36), O/C (CTB: 0.08 and FTB: 0.12), and (O + N)/C (CTB: 0.10 and FTB: 0.12) ratios compared to the TB (H/C = 0.22, O/C = 0.04, and (O + N)/C = 0.06). These results showed that FTB contained relatively less aromatic functional groups than those of TB and CTB [36]. Furthermore CTB and FTB exhibited larger specific surface areas (TB = 9.21 m² g⁻¹; CTB = 342.11 m² g⁻¹; 558.71 m² g⁻¹), larger pore volumes (TB = 0.01 cm³ g⁻¹; CTB = 0.36 cm³ g⁻¹; FTB = 0.18 cm³ g⁻¹), and smaller average pore sizes (TB = 6.07 nm; CTB = 3.67 nm; FTB = 3.64 nm) compared with TB, indicating that activation process with CaCl₂ and FeCl₃ was effective in improving the physicochemical characteristics of the tangerine peel biochars related to PO₄³⁻ adsorption [37].

Table 1. The physicochemical properties of TB, CTB, and FTB.

Properties	TB	CTB	FTB
C (%)	81.12	69.42	53.81
H (%)	1.50	1.94	1.63
O (%)	4.40	7.61	8.39
N (%)	2.09	1.31	1.05
Ash (%)	10.89	19.72	35.12
H/C	0.22	0.34	0.36
O/C	0.04	0.08	0.12
N/C	0.02	0.02	0.02
PO ₄ ³⁻ (mg L ⁻¹) ^a	0.019 ± 0.001	0.047 ± 0.001	0.009 ± 0.002
S _{BET} (m ² g ⁻¹)	9.21	342.11	558.71
Pore volume (cm ³ g ⁻¹)	0.01	0.36	0.18
Pore size (nm)	6.07	3.67	3.64

^a: n = 3.

The functional groups of TB, CTB, and FTB are revealed by FT-IR analysis (Figure 1). The main differences between TB and chemical activated TB (i.e., CTB and FTB) are the

existence of C=O stretching of esters and -COO carboxylates. These functional groups might enhance the adsorption capacities of the phosphate ions using CTB and FTB by working as an electron acceptor [38,39].

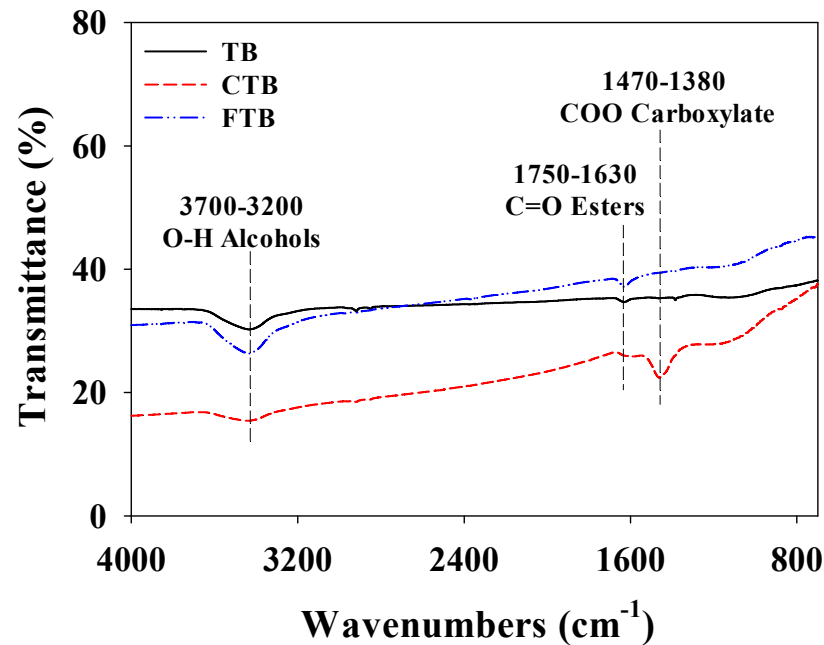


Figure 1. The FT-IR spectra of TB, CTB, and FTB.

3.1.2. UH-SEM-EDX and XRD Analyses

The surfaced morphologies of TB, CTB, and FTB are shown in Figure 2. The surfaces of the CTB (Figure 2b) and FTB (Figure 2c) exhibited much coarser compared to the surface of TB (Figure 2a). These observations are in agreement with the result of measuring the specific surface area using BET. Figure 3 shows the EDX mapping images of the TB, CTB, and FTB surfaces. The surface of TB was mostly composed of carbon (Figure 3a), whereas calcium and iron salts were evenly distributed on the surfaces of CTB and FTB (Figure 3b,c). Moreover, the results of EDX mapping were in good agreement with the atomic percentage of elements in TB, CTB, and FTB (Table 2). These observations indicate that calcium and iron salts were successfully impregnated in the surface of the tangerine peel biochars through pretreatment with CaCl_2 and FeCl_3 .

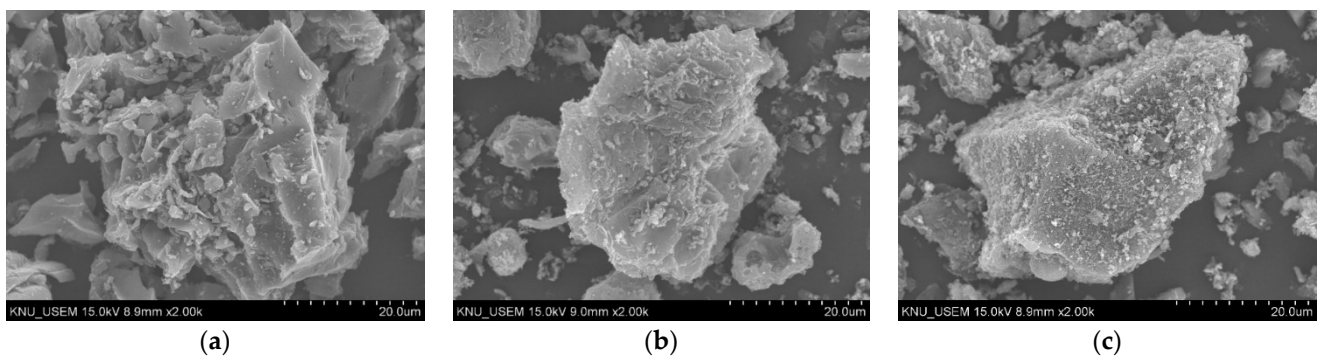


Figure 2. The UH-SEM images of (a) TB; (b) CTB; and (c) FTB.

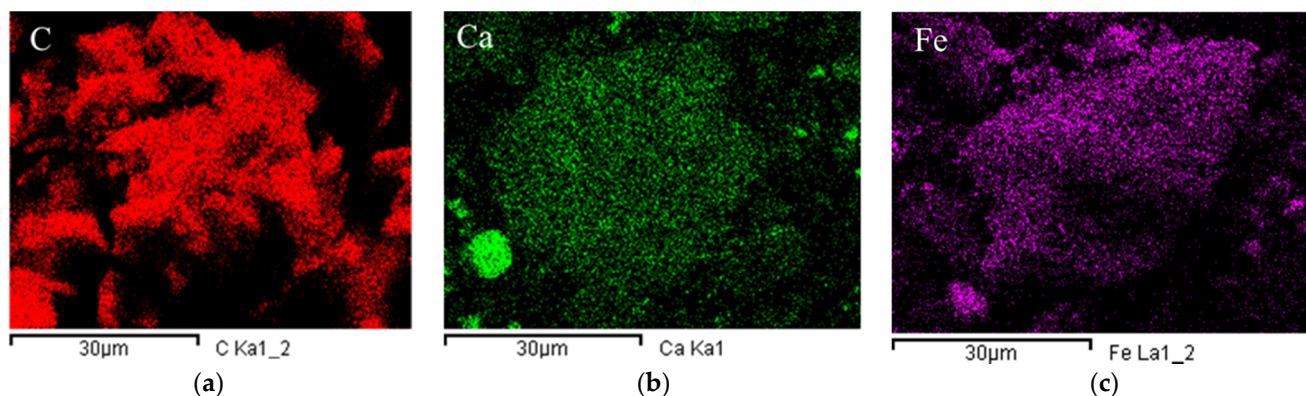


Figure 3. The UH-SEM-EDX mapping of (a) TB; (b) CTB; and (c) FTB (magnification = 2000).

Table 2. Atomic percentage of elements in TB, CTB, and FTB.

Element	Atomic (%)		
	TB	CTB	FTB
C	69.85	55.68	72.26
Ca	29.67	42.71	-
Fe	-	-	21.38
Cl	-	1.61	6.36
Mg	0.48	-	-
Total	100.00	100.00	100.00

The crystallinities of TB, CTB, and FTB were analyzed using XRD (Figure 4). The XRD peaks of TB related to graphite and quartz (SiO_2) were found at $2\theta = 23^\circ$ and 43° , respectively [40]. The XRD peaks of CTB and FTB related to calcium and iron species (e.g., CaCO_3 , MgFe_2O_4) were found (CaCO_3 at $2\theta = 35^\circ, 57^\circ, \text{ and } 65^\circ$; MgFe_2O_4 at $2\theta = 30^\circ, 35^\circ, 43^\circ, 57^\circ, \text{ and } 63^\circ$) [41]. These findings were in good agreement with the SEM-EDX analysis results of TB, CTB, and FTB.

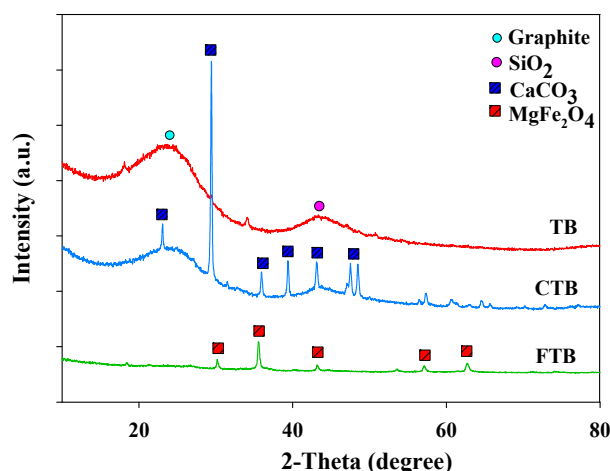


Figure 4. The XRD of TB, CTB, and FTB.

3.2. Effects of Tangerine Peel Biochar Dosage

The adsorbent dosage is one of the critical factors which affect the adsorption of PO_4^{3-} . Figure 5 presents the effects of the dosages of TB, CTB, and FTB on the removal efficiency of PO_4^{3-} . In the case of TB, the removal efficiency of PO_4^{3-} decreased as the adsorbent dosage was increased beyond $0.6 \text{ g}\cdot\text{L}^{-1}$. These results indicated that the decreased adsorption capacity of TB for PO_4^{3-} was caused by reducing the total number of binding sites on

TB surfaces due to the aggregation of TB particles as increasing adsorbent dosage [42]. However, the removal efficiencies of the PO_4^{3-} by CTB and FTB increased with the dosage increase. These results indicated that the activated binding sites of the adsorbents capable of PO_4^{3-} adsorption increased with increasing dosage [43]. Furthermore, FTB was more effective in removing PO_4^{3-} than that of CTB because the binding capacity of iron salts is higher than that of calcium [44]. Based on these experiments on the PO_4^{3-} removal efficiency according to the TB, CTB, and FTB dosages, $0.6 \text{ g}\cdot\text{L}^{-1}$ was selected as the optimal dosage and applied to subsequent experiments.

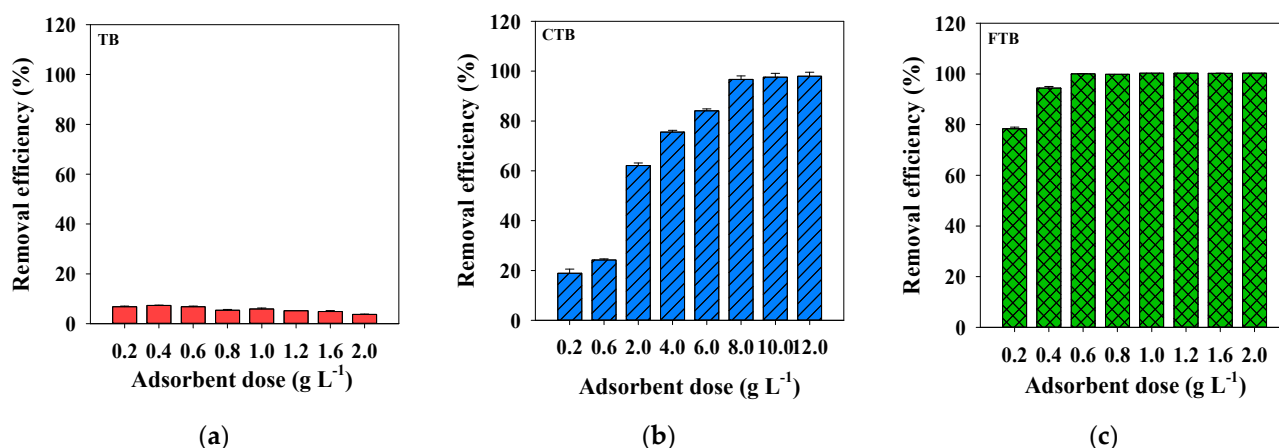


Figure 5. The effects of adsorbent doses on the removal efficiency of PO_4^{3-} by (a) TB, (b) CTB and (c) FTB ($\text{PO}_4^{3-} = 1 \text{ mg}\cdot\text{L}^{-1}$; agitation speed = 150 rpm; temperature = 25 °C; contact time = 24 h; pH = 7.0).

3.3. Adsorption Kinetics

Figure 6 shows the adsorption kinetics of PO_4^{3-} by TB, CTB, and FTB. The adsorption process of PO_4^{3-} is comprised of fast and slow reaction stage. The fast adsorption reaction was completed in about 0.5 h for TB, CTB, and FTB as the activated sites on the surface of the biochars were saturated.

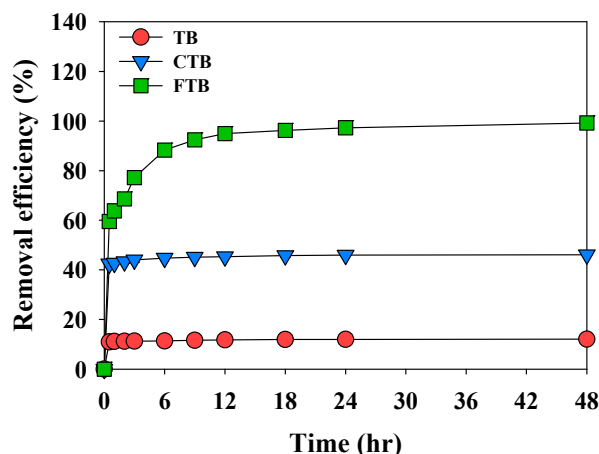


Figure 6. The adsorption kinetics of PO_4^{3-} onto the TB, CTB, FTB (adsorbent dose = $0.6 \text{ g}\cdot\text{L}^{-1}$; $\text{PO}_4^{3-} = 1 \text{ mg}\cdot\text{L}^{-1}$; agitation speed = 150 rpm; temperature = 25 °C; contact time = 24 h; pH = 7).

The fast adsorption reaction was completed in about 0.5 h for TB, CTB, and FTB as the activated sites on the surface of the biochars were saturated. The TB ($Q_{e,exp} = 0.104 \text{ mg}\cdot\text{g}^{-1}$) and CTB ($Q_{e,exp} = 0.354 \text{ mg}\cdot\text{g}^{-1}$) with relatively low removal efficiency compared to FTB, adsorption equilibrium was reached after 2 h. However, the adsorption equilibrium of FTB ($Q_{e,exp} = 1.655 \text{ mg}\cdot\text{g}^{-1}$) was completed in 18 h due to many activated sites on the surface [45]. Table 3 presents the results of calculating the constant and correlation

coefficient of adsorption kinetics. The adsorption of PO_4^{3-} by TB, CTB, and FTB was well fitted for the pseudo-second-order model ($R^2 = 0.999$) than the pseudo-first-order model ($R^2 \geq 0.929$). These results indicated that the adsorption of TB, CTB, and FTB is caused by chemical adsorption [46].

Table 3. The kinetic parameters for the removal of the PO_4^{3-} using TB, CTB, and FTB.

Adsorbents	$Q_{e, exp}$ (mg g^{-1})	Pseudo-First-Order			Pseudo-Second-Order		
		$Q_{e, cal}$ (mg g^{-1})	k_1	R^2	$Q_{e, cal}$ (mg g^{-1})	k_2	R^2
TB	0.104 ± 0.004	0.020 ± 0.002	0.115 ± 0.012	0.990	0.105 ± 0.020	19.73 ± 4.420	0.999
CTB	0.354 ± 0.002	0.103 ± 0.003	0.186 ± 0.012	0.975	0.357 ± 0	5.25 ± 0.620	0.999
FTB	1.655 ± 0.001	0.579 ± 0.001	0.131 ± 0.002	0.929	1.679 ± 0.024	0.734 ± 0.120	0.999

3.4. Adsorption Isotherms

The adsorption behaviors of PO_4^{3-} by the TB, CTB, and FTB were examined using the Langmuir and Freundlich adsorption isotherm models (Table 4). The adsorption of PO_4^{3-} by TB was well fitted to the Freundlich isotherm model with the high R^2 values (R^2 of Langmuir isotherm = 0.887; R^2 of Freundlich isotherm = 0.975). This is evidence that the multilayer adsorption played a critical role in removing the PO_4^{3-} toward the heterogeneous surfaces of the TB [47]. For the CTB and FTB, the adsorption of PO_4^{3-} followed both Langmuir (R^2 of CTB = 0.889; R^2 of FTB = 0.987) and Freundlich (R^2 of CTB = 0.955; R^2 of FTB = 0.912) isotherm models. These observations could explain that the chemical activation with CaCl_2 and FeCl_3 might change the adsorption mechanism (i.e., multilayer adsorption \rightarrow monolayer adsorption) of PO_4^{3-} by the TB. A similar result was previously observed for the removal of the pharmaceuticals with NaOH-activated biochars [48]. The adsorption affinities of PO_4^{3-} to the TB, CTB, and FTB were evaluated using the n values (dimensionless adsorption intensity) of the Freundlich isotherm model: (i) $n > 1.0$ (favorable), (ii) $n = 1.0$ (linear), and (iii) $n < 1.0$ (unfavorable) [49]. The adsorption of PO_4^{3-} by TB (n value = 0.766) was unfavorable, whereas the adsorptions of PO_4^{3-} by CTB (n value = 1.523) and FTB (n value = 7.530) were favorable. The R_L value (maximum adsorption capacity; $R_L = 1/(1 + K_L C_0)$) of the Langmuir isotherm model: (i) $R_L = 0$ (irreversible), (ii) $1 > R_L > 0$ (favorable), (iii) $R_L = 1$ (linear), and (iv) $R_L > 1$ (unfavorable), was assessed to the adsorption affinities of PO_4^{3-} toward TB, CTB, and FTB [50]. The adsorption of PO_4^{3-} by FTB ($R_L = 0.209$) followed the Langmuir isotherm model and seemed to be favorable for the monolayer adsorption [51]. Moreover, these results are comparable to the maximum adsorption capacity (mg g^{-1}) calculated using different adsorbents as shown in Table 5.

Table 4. The isotherm parameters for the removal of the PO_4^{3-} using TB, CTB, and FTB.

Adsorbents	Langmuir			Freundlich		
	Q_{max} (mg g^{-1})	K_L (L mg^{-1})	R^2	n	K_F ($\text{mg}^{1-1/n} \text{L}^{1/n} \text{g}^{-1}$)	R^2
TB	1.540 ± 0.035	0.080 ± 0.004	0.887	0.766 ± 0.022	0.139 ± 0.002	0.975
CTB	3.608 ± 0.011	0.173 ± 0.013	0.889	1.523 ± 0.003	0.539 ± 0.007	0.955
FTB	5.434 ± 0.035	3.786 ± 0.140	0.987	7.530 ± 0.257	3.680 ± 0.084	0.912

Table 5. Summary of available results related to PO_4^{3-} adsorption by biochars.

Biomass	Pyrolysis Temperature (°C)	Application Matrix	Modification Method	Initial Concentration (mg L ⁻¹)	Adsorption Capacity (mg g ⁻¹)	References
Mixed hardwood	300	Aqueous solution	-	24	0.48	[52]
Corn straw	500	Aqueous solution	FeSO ₄	7.5	7.35	[53]
Ground corn	600	Aqueous solution	MgCl ₂	84	7.5	[27]
Cotton stalks	350	Aqueous solution	FeCl ₃	20	0.96	[28]
Tangerine peels	800	Aqueous solution	CaCl ₂ FeCl ₃	1	3.61 5.43	This study

3.5. Effects of pH on Adsorption of PO_4^{3-}

Figure 7 illustrates the effect of pH (pH = 3–9) on the adsorption of PO_4^{3-} using TB, CTB, and FTB. It was presented that the removal efficiency of PO_4^{3-} by TB, CTB, and FTB was not significantly affected by the pH change (removal efficiency of TB = 10.9–12.1%; removal efficiency of CTB = 25.1–29.8%; removal efficiency of FTB = 93.3–99.4%). These results indicated that TB, CTB, and FTB could be used to effectively remove PO_4^{3-} from wastewater with a wide range of pH [54].

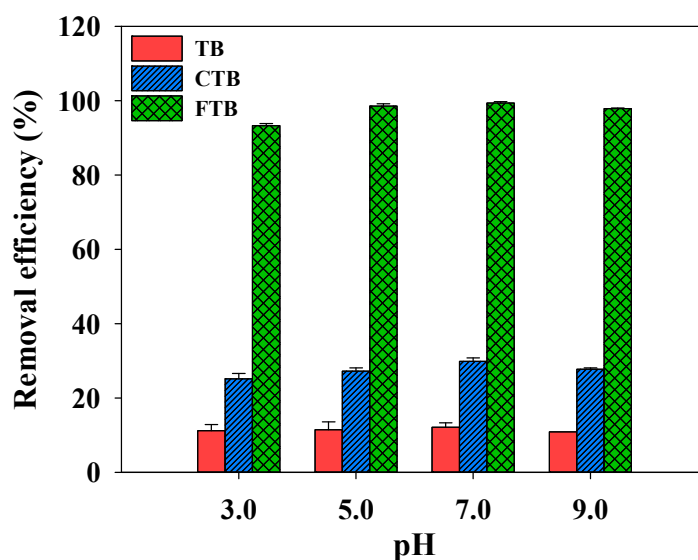


Figure 7. The effects of pH on the removal efficiency of PO_4^{3-} by TB, CTB and FTB (adsorbent dose = 0.6 g L⁻¹; PO_4^{3-} = 1 mg L⁻¹; agitation speed = 150 rpm; temperature = 25 °C; contact time = 24 h).

3.6. Effects of Ionic Strength on Adsorption of PO_4^{3-}

The effects of ionic strength (ionic strength = 0–0.5 M) on the adsorption of PO_4^{3-} by TB, CTB, and FTB are shown in Figure 8. The removal efficiency of PO_4^{3-} by TB was not significantly affected by the ionic strength change (the removal efficiency of PO_4^{3-} = 9.7%→10.5%). However, the removal efficiencies of PO_4^{3-} using the CTB and FTB were gradually decreased with increasing ionic strengths (CTB: the removal efficiency of PO_4^{3-} = 25.2%→14.8%; FTB: the removal efficiency of PO_4^{3-} = 98.8%→55.1%). These observations suggested that increases in ionic strength might reinforce the electrostatic repulsion between PO_4^{3-} and adsorbent surfaces, and activated adsorption sites on the surface might be reduced due to the compression of the electrical double layer on the adsorbent surfaces [55].

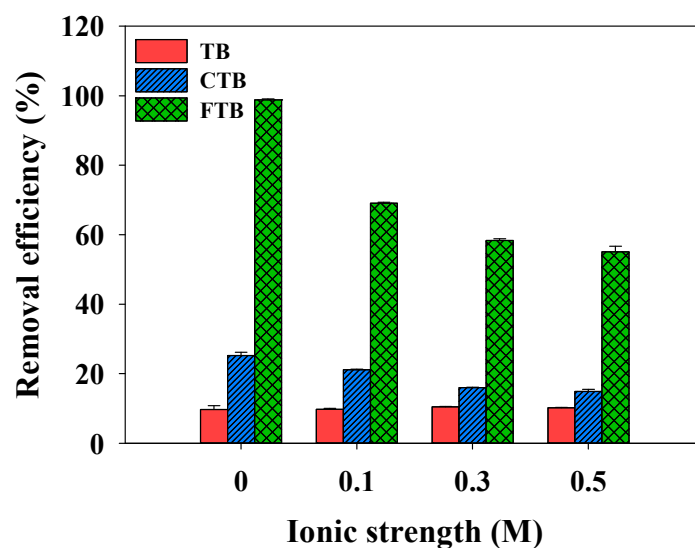


Figure 8. The effects of ionic strength on the removal efficiency of PO₄³⁻ by TB, CTB and FTB (adsorbent doses = 0.6 g L⁻¹; PO₄³⁻ = 1 mg L⁻¹; agitation speed = 150 rpm; contact time = 24 h; pH = 7.0).

3.7. Effects of Temperature and Thermodynamic Analysis

The effects of the temperature on the removal efficiencies of the PO₄³⁻ by TB, CTB, and FTB are compared in Figure 9 (temperature = 15–35 °C). The adsorption of PO₄³⁻ on the CTB gradually increased with increasing temperature (Figure 9, the removal efficiency of CTB = 18.2%→37.5%). A possible explanation for these results is that increasing temperature cause more strong intermolecular motion and PO₄³⁻ diffusion rate to the surface of CTB, which promoted the adsorption of PO₄³⁻ on the CTB [56]. However, the removal efficiencies of PO₄³⁻ by TB and FTB were not significantly affected by the temperature change (removal efficiency of TB = 7.3–7.9%; removal efficiency of FTB = 98.2–100.0%). Table 6 shows the values of the thermodynamic parameters (ΔG° , ΔH° , and ΔS°) for PO₄³⁻ removal by TB, CTB, and FTB according to the temperature (15–35 °C). The $\Delta G^\circ < 0$ and $\Delta H^\circ > 0$ suggested that the adsorption of PO₄³⁻ on the TB, CTB, and FTB was a spontaneous and endothermic reaction [57,58]. Furthermore, $\Delta S^\circ > 0$ indicated that the adsorption of PO₄³⁻ on the TB, CTB, and FTB was irreversible, which was conducive to the adsorption stability [56].

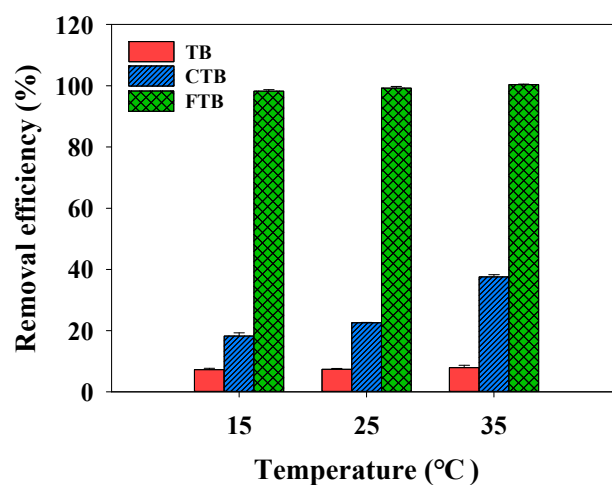


Figure 9. The effects of temperature on the removal efficiency of PO₄³⁻ by TB, CTB and FTB (adsorbent doses = 0.6 g L⁻¹; PO₄³⁻ = 1 mg L⁻¹; agitation speed = 150 rpm; contact time = 24 h; pH = 7.0).

Table 6. The thermodynamic parameters of PO₄^{3−} adsorption onto TB, CTB, and FTB.

Adsorbents	Thermodynamic Parameters			
	Temperature (K)	ΔG° (kJ mol ^{−1})	ΔH° (kJ mol ^{−1})	ΔS° (J mol ^{−1} K)
TB	288	−11.650 ±0.311	0.016 ±0.001	0.024 ±0.005
	298	−12.082 ±0.111		
	308	−12.704 ±0.241		
CTB	288	−14.161 ±0.168	0.001 ±0.0005	0.107 ±0.001
	298	−15.322 ±0.014		
	308	−17.688 ±0.074		
FTB	288	−18.996 ±0.321	0.001 ±0.0008	0.039 ±0.015
	298	−27.330 ±0.713		
	308	−30.418 ±1.782		

4. Conclusions

This study verified that pretreatment with CaCl₂ and FeCl₃ could improve the surface characteristics of tangerine peel biochars related to the adsorption behaviors of PO₄^{3−}. The FTB might more effectively remove the PO₄^{3−} (Q_{e, exp} = 1.655 mg g^{−1}) than TB (Q_{e, exp} = 0.104 mg g^{−1}) and CTB (Q_{e, exp} = 0.354 mg g^{−1}) due to the considerable enhancement of the physicochemical characteristics (specific surface area and surface characteristics). The removal efficiencies of PO₄^{3−} by TB (R² = 0.975) and CTB (R² = 0.955) were more suitable for the Freundlich adsorption model (multilayer adsorption) and the FTB was well fitted to the Langmuir adsorption model (R² = 0.987, monolayer adsorption). Furthermore, the thermodynamic analysis presented that the adsorption of PO₄^{3−} for the FTB was more spontaneously endothermic than that for the TB and CTB under various pH and ionic strength conditions. These results are evidence that the chemical activation with FeCl₃ might be a promising option to make the pristine tangerine peel biochar practically more relevant for the removal of PO₄^{3−} in the aqueous solutions.

Author Contributions: Conceptualization, C.S.; methodology, W.A.; validation, I.J.; formal analysis, G.L.; data curation, C.S.; writing—original draft preparation, C.S.; writing—review and editing, Y.-G.L. and K.C.; supervision, K.C.; funding acquisition, Y.-G.L. All authors have read and agreed to the published version of the manuscript.

Funding: This research was supported by Basic Science Research Program through the National Research Foundation of Korea (NRF) funded by the Ministry of Education (NRF-2020R111A1A01073157).

Conflicts of Interest: The authors declare no conflict of interest.

References

1. Kılıc, M.; Kırbıyık, C.; Çepelioğullar, Ö.; Pütün, A.E. Adsorption of heavy metal ions from aqueous solutions by bio-char, a by-product of pyrolysis. *Appl. Surf. Sci.* **2013**, *283*, 856–862. [[CrossRef](#)]
2. Bishop, M.J.; Powers, S.P.; Porter, H.J.; Peterson, C.H. Benthic biological effects of seasonal hypoxia in a eutrophic estuary predate rapid coastal development. *Estuar. Coast. Shelf Sci.* **2006**, *70*, 415–422. [[CrossRef](#)]
3. Withers, P.J.; Neal, C.; Jarvie, H.P.; Doody, D.G. Agriculture and eutrophication: Where do we go from here? *Sustainability* **2014**, *6*, 5853–5875. [[CrossRef](#)]
4. Carpenter, S.R.; Caraco, N.F.; Correll, D.L.; Howarth, R.W.; Sharpley, A.N.; Smith, V.H. Nonpoint pollution of surface waters with phosphorus and nitrogen. *Ecol. Appl.* **1998**, *8*, 559–568. [[CrossRef](#)]

5. Bennett, E.M.; Carpenter, S.R.; Caraco, N.F. Human impact on erodable phosphorus and eutrophication: A global perspective: Increasing accumulation of phosphorus in soil threatens rivers, lakes, and coastal oceans with eutrophication. *BioScience* **2001**, *51*, 227–234. [[CrossRef](#)]
6. Oguz, E. Thermodynamic and kinetic investigations of PO₃–4 adsorption on blast furnace slag. *J. Colloid Interface Sci.* **2005**, *281*, 62–67. [[CrossRef](#)] [[PubMed](#)]
7. Chubar, N.; Kanibolotsky, V.; Strelko, V.; Gallios, G.; Samanidou, V.; Shaposhnikova, T.; Milgrandt, V.; Zhuravlev, I. Adsorption of phosphate ions on novel inorganic ion exchangers. *Colloids Surf. A Physicochem. Eng. Asp.* **2005**, *255*, 55–63. [[CrossRef](#)]
8. Abu-Alhail, S.; Lu, X.W. Experimental investigation and modeling of innovative five-tank anaerobic-anoxic/oxic process. *Appl. Math. Model.* **2014**, *38*, 278–290. [[CrossRef](#)]
9. Mohan, D.; Pittman, C.U., Jr. Arsenic removal from water/wastewater using adsorbents—A critical review. *J. Hazard. Mater.* **2007**, *142*, 1–53. [[CrossRef](#)]
10. Seida, Y.; Nakano, Y. Removal of phosphate by layered double hydroxides containing iron. *Water Res.* **2002**, *36*, 1306–1312. [[CrossRef](#)]
11. Zhang, L.; Xu, C.; Champagne, P.; Mabee, W. Overview of current biological and thermo-chemical treatment technologies for sustainable sludge management. *Waste Manag. Res.* **2014**, *32*, 586–600. [[CrossRef](#)] [[PubMed](#)]
12. Ayrançi, E.; Hoda, N. Adsorption of bentazon and propanil from aqueous solutions at the high area activated carbon-cloth. *Chemosphere* **2004**, *57*, 755–762. [[CrossRef](#)] [[PubMed](#)]
13. Das, J.; Patra, B.S.; Baliarsingh, N.; Parida, K.M. Adsorption of phosphate by layered double hydroxides in aqueous solutions. *Appl. Clay Sci.* **2006**, *32*, 252–260. [[CrossRef](#)]
14. Chen, J.; Kong, H.; Wu, D.; Chen, X.; Zhang, D.; Sun, Z. Phosphate immobilization from aqueous solution by fly ashes in relation to their composition. *J. Hazard. Mater.* **2007**, *139*, 293–300. [[CrossRef](#)]
15. Zhang, L.; Wan, L.; Chang, N.; Liu, J.; Duan, C.; Zhou, Q.; Li, X.; Wang, X. Removal of phosphate from water by activated carbon fiber loaded with lanthanum oxide. *J. Hazard. Mater.* **2011**, *190*, 848–855. [[CrossRef](#)] [[PubMed](#)]
16. Yuan, M.; Tong, S.; Zhao, S.; Jia, C.Q. Adsorption of polycyclic aromatic hydrocarbons from water using petroleum coke-derived porous carbon. *J. Hazard. Mater.* **2010**, *181*, 1115–1120. [[CrossRef](#)]
17. Yin, Q.; Ren, H.; Wang, R.; Zhao, Z. Evaluation of nitrate and phosphate adsorption on Al-modified biochar: Influence of Al content. *Sci. Total Environ.* **2018**, *631–632*, 895–903. [[CrossRef](#)]
18. Yao, Y.; Gao, B.; Zhang, M.; Inyang, M.; Zimmerman, A.R. Effect of biochar amendment on sorption and leaching of nitrate, ammonium, and phosphate in a sandy soil. *Chemosphere* **2012**, *89*, 1467–1471. [[CrossRef](#)]
19. Zhou, Y.; Gao, B.; Zimmerman, A.R.; Chen, H.; Zhang, M.; Cao, X. Biochar-supported zerovalent iron for removal of various contaminants from aqueous solutions. *Bioresour. Technol.* **2014**, *152*, 538–542. [[CrossRef](#)]
20. Kim, Y.-M.; Lee, H.W.; Lee, S.-H.; Kim, S.-S.; Park, S.H.; Jeon, J.-K.; Kim, S.; Park, Y.-K. Pyrolysis properties and kinetics of mandarin peel. *Korean J. Chem. Eng.* **2011**, *28*, 2012–2016. [[CrossRef](#)]
21. Biswas, B.K.; Inoue, J.-i.; Inoue, K.; Ghimire, K.N.; Harada, H.; Ohto, K.; Kawakita, H. Adsorptive removal of As(V) and As(III) from water by a Zr(IV)-loaded orange waste gel. *J. Hazard. Mater.* **2008**, *154*, 1066–1074. [[CrossRef](#)]
22. Li, X.; Tang, Y.; Cao, X.; Lu, D.; Luo, F.; Shao, W. Preparation and evaluation of orange peel cellulose adsorbents for effective removal of cadmium, zinc, cobalt and nickel. *Colloids Surf. A Physicochem. Eng. Asp.* **2008**, *317*, 512–521. [[CrossRef](#)]
23. Chen, B.; Chen, Z.; Lv, S. A novel magnetic biochar efficiently sorbs organic pollutants and phosphate. *Bioresour. Technol.* **2011**, *102*, 716–723. [[CrossRef](#)] [[PubMed](#)]
24. Zhang, M.; Gao, B. Removal of arsenic, methylene blue, and phosphate by biochar/AlOOH nanocomposite. *Chem. Eng. J.* **2013**, *226*, 286–292. [[CrossRef](#)]
25. Yao, Y.; Gao, B.; Chen, J.; Yang, L. Engineered biochar reclaiming phosphate from aqueous solutions: Mechanisms and potential application as a slow-release fertilizer. *Environ. Sci. Technol.* **2013**, *47*, 8700–8708. [[CrossRef](#)] [[PubMed](#)]
26. Choi, Y.-K.; Jang, H.M.; Kan, E.; Wallace, A.R.; Sun, W. Adsorption of phosphate in water on a novel calcium hydroxide-coated dairy manure-derived biochar. *Environ. Eng. Res.* **2019**, *24*, 434–442. [[CrossRef](#)]
27. Fang, C.; Zhang, T.; Li, P.; Jiang, R.-f.; Wang, Y.-c. Application of magnesium modified corn biochar for phosphorus removal and recovery from swine wastewater. *Int. J. Environ. Res. Public Health* **2014**, *11*, 9217–9237. [[CrossRef](#)] [[PubMed](#)]
28. Ren, J.; Li, N.; Li, L.; An, J.-K.; Zhao, L.; Ren, N.-Q. Granulation and ferric oxides loading enable biochar derived from cotton stalk to remove phosphate from water. *Bioresour. Technol.* **2015**, *178*, 119–125. [[CrossRef](#)]
29. Qian, L.; Zhang, W.; Yan, J.; Han, L.; Gao, W.; Liu, R.; Chen, M. Effective removal of heavy metal by biochar colloids under different pyrolysis temperatures. *Bioresour. Technol.* **2016**, *206*, 217–224. [[CrossRef](#)] [[PubMed](#)]
30. Towns, T.G. Determination of aqueous phosphate by ascorbic acid reduction of phosphomolybdic acid. *Anal. Chem.* **1986**, *58*, 223–229. [[CrossRef](#)]
31. Bhainsa, K.C.; D’souza, S. Removal of copper ions by the filamentous fungus, *Rhizopus oryzae* from aqueous solution. *Bioresour. Technol.* **2008**, *99*, 3829–3835. [[CrossRef](#)]
32. Gorgievski, M.; Božić, D.; Stanković, V.; Štrbac, N.; Šerbula, S. Kinetics, equilibrium and mechanism of Cu²⁺, Ni²⁺ and Zn²⁺ ions biosorption using wheat straw. *Ecol. Eng.* **2013**, *58*, 113–122. [[CrossRef](#)]
33. Lee, J.-J. Study on equilibrium, kinetic and thermodynamic for adsorption of quinoline yellow by granular activated carbon. *Clean Technol.* **2014**, *20*, 35–41. [[CrossRef](#)]

34. Chen, S.; Qin, C.; Wang, T.; Chen, F.; Li, X.; Hou, H.; Zhou, M. Study on the adsorption of dyestuffs with different properties by sludge-rice husk biochar: Adsorption capacity, isotherm, kinetic, thermodynamics and mechanism. *J. Mol. Liq.* **2019**, *285*, 62–74. [[CrossRef](#)]
35. Li, M.; Zhao, Z.; Wu, X.; Zhou, W.; Zhu, L. Impact of mineral components in cow manure biochars on the adsorption and competitive adsorption of oxytetracycline and carbaryl. *RSC Adv.* **2017**, *7*, 2127–2136. [[CrossRef](#)]
36. Luo, L.; Wang, G.; Shi, G.; Zhang, M.; Zhang, J.; He, J.; Xiao, Y.; Tian, D.; Zhang, Y.; Deng, S. The characterization of biochars derived from rice straw and swine manure, and their potential and risk in N and P removal from water. *J. Environ. Manag.* **2019**, *245*, 1–7. [[CrossRef](#)]
37. Liu, J.; Zhou, Q.; Chen, J.; Zhang, L.; Chang, N. Phosphate adsorption on hydroxyl-iron-lanthanum doped activated carbon fiber. *Chem. Eng. J.* **2013**, *215*, 859–867. [[CrossRef](#)]
38. Zhao, J.; Shen, X.-J.; Domene, X.; Alcañiz, J.-M.; Liao, X.; Palet, C. Comparison of biochars derived from different types of feedstock and their potential for heavy metal removal in multiple-metal solutions. *Sci. Rep.* **2019**, *9*, 9869. [[CrossRef](#)]
39. Binda, G.; Spanu, D.; Bettinetti, R.; Magagnin, L.; Pozzi, A.; Dossi, C. Comprehensive comparison of microalgae-derived biochar from different feedstocks: A prospective study for future environmental applications. *Algal Res.* **2020**, *52*, 102103. [[CrossRef](#)]
40. Wang, S.; Zhao, C.; Shan, R.; Wang, Y.; Yuan, H. A novel peat biochar supported catalyst for the transesterification reaction. *Energy Convers. Manag.* **2017**, *139*, 89–96. [[CrossRef](#)]
41. Shakir, I.; Sarfraz, M.; Ali, Z.; Aboud, M.F.; Agboola, P.O. Magnetically separable and recyclable graphene-MgFe₂O₄ nanocomposites for enhanced photocatalytic applications. *J. Alloy Compd.* **2016**, *660*, 450–455. [[CrossRef](#)]
42. Banerjee, S.; Mukherjee, S.; LaminKa-ot, A.; Joshi, S.R.; Mandal, T.; Halder, G. Biosorptive uptake of Fe²⁺, Cu²⁺ and As⁵⁺ by activated biochar derived from *Colocasia esculenta*: Isotherm, kinetics, thermodynamics, and cost estimation. *J. Adv. Res.* **2016**, *7*, 597–610. [[CrossRef](#)]
43. Almasi, A.; Omidi, M.; Khodadadian, M.; Khamutian, R.; Gholivand, M.B. Lead (II) and cadmium (II) removal from aqueous solution using processed Walnut shell: Kinetic and equilibrium study. *Toxicol. Environ. Chem.* **2012**, *94*, 660–671. [[CrossRef](#)]
44. Yan, H.; Shih, K. Effects of calcium and ferric ions on struvite precipitation: A new assessment based on quantitative X-ray diffraction analysis. *Water Res.* **2016**, *95*, 310–318. [[CrossRef](#)]
45. Pellera, F.-M.; Giannis, A.; Kalderis, D.; Anastasiadou, K.; Stegmann, R.; Wang, J.-Y.; Gidaracos, E. Adsorption of Cu (II) ions from aqueous solutions on biochars prepared from agricultural by-products. *J. Environ. Manag.* **2012**, *96*, 35–42. [[CrossRef](#)]
46. Mistar, E.; Ahmad, S.; Muslim, A.; Alfatah, T.; Supardan, M. Preparation and characterization of a high surface area of activated carbon from *Bambusa vulgaris*—Effect of NaOH activation and pyrolysis temperature. In Proceedings of the 3rd International Conference on Chemical Engineering Sciences and Applications 2017, Banda Aceh, Indonesia, 20–21 September 2017.
47. Lee, K.-H.; Lee, Y.-G.; Shin, J.; Chon, K.; Lee, S.-H. Selective immobilization of antimony using brucite-rich precipitate produced during in situ hypochlorous acid formation through seawater electrolysis in a nuclear power plant. *Energies* **2020**, *13*, 4493. [[CrossRef](#)]
48. Shin, J.; Kwak, J.; Lee, Y.-G.; Kim, S.; Choi, M.; Bae, S.; Lee, S.-H.; Park, Y.; Chon, K. Competitive adsorption of pharmaceuticals in lake water and wastewater effluent by pristine and NaOH-activated biochars from spent coffee wastes: Contribution of hydrophobic and π - π interactions. *Environ. Pollut.* **2021**, *270*, 116244. [[CrossRef](#)]
49. Kim, H.; Ko, R.-A.; Lee, S.; Chon, K. Removal efficiencies of manganese and iron using pristine and phosphoric acid pre-treated biochars made from banana peels. *Water* **2020**, *12*, 1173. [[CrossRef](#)]
50. Hayati, B.; Mahmoodi, N.M. Modification of activated carbon by the alkaline treatment to remove the dyes from wastewater: Mechanism, isotherm and kinetic. *Desalination Water Treat.* **2012**, *47*, 322–333. [[CrossRef](#)]
51. Zhou, N.; Chen, H.; Xi, J.; Yao, D.; Zhou, Z.; Tian, Y.; Lu, X. Biochars with excellent Pb (II) adsorption property produced from fresh and dehydrated banana peels via hydrothermal carbonization. *Bioresour. Technol.* **2017**, *232*, 204–210. [[CrossRef](#)]
52. Sarkhot, D.V.; Ghezzehei, T.A.; Berhe, A.A. Effectiveness of biochar for sorption of ammonium and phosphate from dairy effluent. *J. Environ. Qual.* **2013**, *42*, 1545–1554. [[CrossRef](#)]
53. Liu, F.; Zuo, J.; Chi, T.; Wang, P.; Yang, B. Removing phosphorus from aqueous solutions by using iron-modified corn straw biochar. *Front. Environ. Sci. Eng.* **2015**, *9*, 1066–1075. [[CrossRef](#)]
54. Ma, Y.; Liu, W.-J.; Zhang, N.; Li, Y.-S.; Jiang, H.; Sheng, G.-P. Polyethylenimine modified biochar adsorbent for hexavalent chromium removal from the aqueous solution. *Bioresour. Technol.* **2014**, *169*, 403–408. [[CrossRef](#)]
55. Behera, S.; Oh, S.; Park, H. Sorptive removal of ibuprofen from water using selected soil minerals and activated carbon. *Int. J. Environ. Sci. Technol.* **2012**, *9*, 85–94. [[CrossRef](#)]
56. Yan, L.; Liu, Y.; Zhang, Y.; Liu, S.; Wang, C.; Chen, W.; Liu, C.; Chen, Z.; Zhang, Y. ZnCl₂ modified biochar derived from aerobic granular sludge for developed microporosity and enhanced adsorption to tetracycline. *Bioresour. Technol.* **2020**, *297*, 122381. [[CrossRef](#)]
57. Dai, Y.; Zhang, K.; Meng, X.; Li, J.; Guan, X.; Sun, Q.; Sun, Y.; Wang, W.; Lin, M.; Liu, M.; et al. New use for spent coffee ground as an adsorbent for tetracycline removal in water. *Chemosphere* **2019**, *215*, 163–172. [[CrossRef](#)] [[PubMed](#)]
58. Wang, B.; Jiang, Y.-s.; Li, F.-y.; Yang, D.-y. Preparation of biochar by simultaneous carbonization, magnetization and activation for norfloxacin removal in water. *Bioresour. Technol.* **2017**, *233*, 159–165. [[CrossRef](#)] [[PubMed](#)]